INVESTIGATION OF THE FLUORESCENCE QUENCHING DEPENDING ON EXCITATION WAVELENGTHS OF RHODAMINE B TO QUANTIFY SILVER NANOPARTICLES VIA THE INNER FILTER EFFECT

Tran Thu Trang
TNU - University of Sciences

ARTICLE INFO

Received: 17/01/2024
Revised: 25/3//2024
Published: 25/3//2024

KEYWORDS

Silver nanoparticles
Rhodamine B
Fluorescence quenching
Inner filter effect (IFE)
Quantification of silver nanoparticles

ABSTRACT

Silver nanoparticles (Ag NPs) with a size of around 9 nm were fabricated and quantified through fluorescence quenching of rhodamine B (RhB). A series of solutions composed of RhB with various concentrations of Ag NPs ranging from 0.09 pM to 0.98 pM were prepared, and optical properties were investigated by absorption and fluorescence spectroscopies. The fluorescence quenching of RhB was observed for the mixing solution of RhB and Ag NPs. The fluorescence measurement condition was optimized by controlling excitation wavelengths to obtain the highest efficiency of fluorescence quenching. The examination of the fluorescence quenching depending on excitation wavelengths indicated that under the excitation wavelength of 400 nm, the highest efficiency of fluorescence quenching of RhB was achieved. At this optimized condition, the lowest concentration of Ag NPs that could be quantified reaches 0.09 pM. It shows a good limitation in the detection of Ag NPs in comparison with the previous works. The mechanism of fluorescence quenching of RhB with the presence of Ag NPs has been revealed as the result of the inner filter effect.

NGHIÊN CỨU SỰ DẬP TẮT HUỲNH QUANG CỦA RHODAMINE B PHỤ THUỘC VÀO BƯỚC SÓNG KÍCH THÍCH ĐỂ ĐỊNH LƯỢNG HẠT NANO BẠC THÔNG QUA HIỆU ỨNG NỘI DẬP TẮT

Trần Thu Trang
Trường Đại học Khoa học - ĐH Thái Nguyên

THÔNG TIN BÀI BÁO

Ngày nhận bài: 17/01/2024
Ngày hoàn thiện: 25/3//2024
Ngày đăng: 25/3//2024

TỪ KHÓA

Hạt nano bạc
Rhodamine B
Dập tắt huỳnh quang
Hiệu ứng inner filter effect
Định lượng nano bạc

TÓM TẮT

Hạt nano bạc (Ag NPs) kích thước khoảng 9 nm đã được tổng hợp và nghiên cứu định lượng thông qua sự dập tắt huỳnh quang của phân tử màu rhodamine B (RhB). Một hệ các dung dịch bao gồm RhB và Ag NPs với nồng độ Ag NPs thay đổi từ 0,09 pM đến 0,98 pM đã được chuẩn bị và nghiên cứu tính chất quang bằng phổ hấp thụ và phổ huỳnh quang. Sự dập tắt huỳnh quang của RhB đã quan sát được trong các hệ dụng dịch Ag NPs và RhB. Điều kiện đo phổ huỳnh quang đã được tối ưu để thu được hiệu suất dập tắt huỳnh quang cao nhất. Qua khảo sát sự dập tắt huỳnh quang phụ thuộc vào các bước sóng kích thích khác nhau đã cho thấy hiệu suất dập tắt huỳnh quang xảy ra cao nhất khi kích thích ở bước sóng 400 nm. Ở điều kiện kích thích 400 nm, nồng độ Ag NPs thấp nhất để có thể phát hiện được đạt tới 0,09 pM. Đây là giới hạn phát hiện Ag NPs tốt so với các công bố trước. Cơ chế của sự dập tắt huỳnh quang được chỉ ra là do hiện tượng nội dập tắt (Inner filter effect).

DOI: https://doi.org/10.34238/tnu-jst.9606

Email: trangtt@tnus.edu.vn

1. Introduction

Fluorescence quenching is one of the most common techniques that has been used in chemical sensing and biosensing [1], [2]. At first, fluorescence quenching due to the inner filter effect was considered an error. The primary inner filter effect describes a quenching of fluorescence due to the attenuation of the excitation beam, and the secondary inner filter effect presents the reabsorption of the emitted radiation by absorbers [3], [4]. The significant changes in fluorescence intensity correlated to the different concentrations of analyte can be exploited as a sensor. Moreover, the slight changes in concentration of the absorber are inferred into exponential changes in the fluorescence signal, making the advantage of fluorescence in detecting low concentrations of analytes.

Silver nanoparticles (Ag NPs) possess a high extinction coefficient in the order of 10^8 $cm^{-1}M^{-1}$ or even more, which is much larger than conventional absorbers [5]. Additionally, the surface plasmon absorption of Ag NPs can be easily turned by controlling their size, shape, or environment [6], [7]. Analytical methods for quantification of silver nanoparticles, in particular, and metal nanoparticles, in general, are still inadequately studied. Pacioni et al. reported quantifying silver and gold nanoparticles using rhodamine 6G [8]. Rhodamin 6G and 4-hydroxycoumarin were also used to study fluorescence quenching with the presence of silver nanoparticles [9]. These previous works concluded that Froster energy transfer played an essential role in the quenching mechanism. Fluorescence sensing based on the inner filter effect (EFE) has currently been explored as a simple approach for detection in various analytics. Cayuela et al. have detected silver nanoparticles in cosmetics by fluorescence quenching of cacbon dots through the IFE mechanism [10].

In this report, Ag NPs were synthesized and quantified through the fluorescence quenching of the fluorophore - Rhodamine B (labeled as RhB). Upon examination of various excitation wavelengths, the Ag NPs and RhB system revealed that the most efficient fluorescence quenching was under excitation wavelength at 400 nm. The lowest concentration of Ag NPs in which the photosystems of Ag NPs and RhB are still detected reaches 0.09 pM. It was deduced that the inner filter effect acted as the crucial mechanism of fluorescence quenching of RhB with the presence of RhB. The study indicated a good of limited detection of Ag NPs through fluorescence quenching of RhB.

2. Materials and methods

2.1. Materials

Silver nitrate ($AgNO_3$, 99.92%) was used as silver precursor; sodium borohydride ($NaBH_4$, 99.9%) acted as both reducing and capping agents. Trisodium citrate dihydrate (TSC, 99%) was also used as a reducing chemical; sodium hydroxide (NaOH, 99%), rhodamine B (RhB, Aldrich). All experiments used deionized water from a Millipore purification system for solution preparation.

2.2. Chemical synthesis of silver nanoparticles

Silver nanoparticles were synthesized by the reduction process of $AgNO_3$ by $NaBH_4$. The formation of silver nanoparticles started with a simple aqueous phase mixing of $AgNO_3$ with TCS and $NaBH_4$ [11], [12]. Briefly, a mixture of 2 ml $AgNO_3$ (0.02 M), 400 µl TSC (0.6 M), and 200 ml deionized water was magnetically stirred at room temperature for 15 minutes. Next, 800 µl of $NaBH_4$ was added dropwise to the mixture. Finally, 200 µl of NaOH (1M) was added to the solution. Following that, the whole mixture was magnetically stirred for 15 minutes. The solution changed the color to yellow-brown, indicating the formation of Ag NPs.

2.3. Instrumentation

Absorption spectra were carried out using a UV-Vis spectrometer (Jasco V-770, Japan). The fluorescence spectra were implemented in fluorescence spectroscopy (model FLS 1000, Scotland). The excitation wavelengths were chosen at 349, 370, 400, 430, 480, 510, and 530 nm. The measurements for each solution were kept under the same conditions for each excitation wavelength.

The morphology of Ag NPs was examined using a transmission electron microscope (TEM) and high-resolution transmission electron microscopy (HRTEM). The crystal structure was investigated by X-ray powder diffraction (XRD) using monochromatic Cu-K_α radiation on a Bruker D8 Advances diffractometer (Germany).

3. Results and discussion

3.1. Morphology and crystal structure of silver nanoparticles

Firstly, the morphology and size of as-synthesized silver nanoparticles (Ag NPs) were examined by using TEM and HRTEM, as indicated in Figure 1. Figure 1a presents that Ag NPs are mostly spherical. The distance between adjacent lattice fringers of Ag was determined using HRTEM and indicated approximately 0.234 nm (Figure 1b). This result is consistent with the (111) plane of silver, and the continuous fringe pattern obtained in the HRTEM image evidences the single crystalline nature of silver NPs [13], [14]. Furthermore, the absorption spectrum of silver NPs (Figure 1c) shows the characteristic band at 399 nm. The morphology of Ag NPs was again strengthened with the characteristic of absorption band at 399 nm. This absorption band stems from the localized surface plasmon band of spherical silver NP_S with an average diameter range of about 10 nm [13], [15], [16].

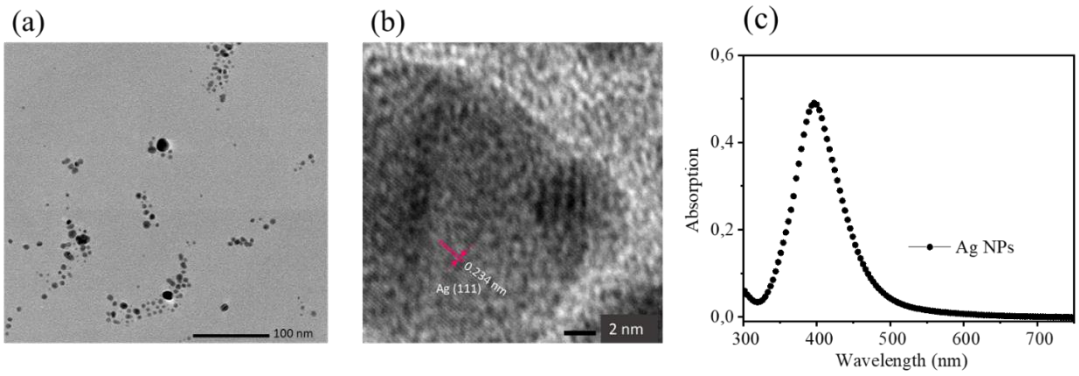

Figure 1. *(a) TEM and (b) HRTEM images of Ag NPs; (c) absorption spectrum of silver NPs*

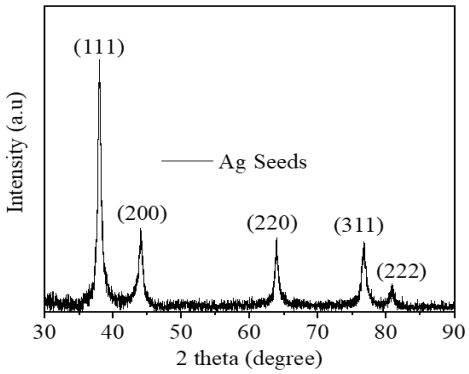

Figure 2. *XRD pattern of silver nanoparticles*

In order to reinforce the structure of silver NPs, XRD measurement was implemented. As presented in Figure 2, all the peaks which are observed at $2\theta = 37.9^0$, 44^0, 63.3^0, and 76.7^0 are identified as the characteristic diffraction peaks of the face-centered cubic structure of silver (JCPDS card no. 04-0783) [17]. Therefore, the results describe the high purity and crystallization of silver NPs.

3.2. Rhodamine B as a fluorescence sensor for silver NPs detection

3.2.1. Absorption spectra study

In order to investigate the ability to detect Ag NPs by RhB, firstly, a series of samples composed of Ag NPs and RhB in aqueous solution were prepared with the concentration of Ag NPs varying from 0.09 pM to 0.98 pM. Because Ag NPs solution is completely dispersed and homogeneous, the concentration of Ag NPs was approximately estimated using Beer-Lambert law: $A = \varepsilon \times L \times C$; in which ε is molar extinction coefficient ($mol^{-1}.cm^{-1}$); L path length (cm), in this case, is the width of cuvet (1 cm); and C is concentration (mol); and A is optical density obtained from absorption spectra of Ag NPs (Figure 3a). In this work, the extinction coefficient of Ag NPs is about 5.5×10^8 ($mol^{-1}.cm^{-1}$) [16]. For an instant to calculate the concentration of Ag NPs corresponds to A = 0.5; $C = A/(\varepsilon \times L) = 0.5/(5.5 \times 10^8 \times 1) = 0.98 \times 10^{-9}$ M = 0.98 pM. Figure 3 describes the absorption spectra of Ag NPs and Ag NPs with a fixed concentration of RhB at 0.5 µM. The inset figure is the absorption spectrum of RhB (0.5 µM) in water with a center band at 553 nm. The concentration of RhB was chosen at 0.5 µM with the purpose of keeping its optical density lower than 0.1, which is the value providing reliable fluorescent signals [3]. In addition to that, the lower concentration of fluorophore corresponds to the higher sensitivity with the presence of an absorber. In Figure 3, it is clear that the absorption spectra of the mixing solution of Ag NPs and RhB describe the overall characteristics of the two components of the absorption spectra of Ag NPs (centered at 399 nm) and RhB (centered at 553 nm). Thus, it could be deduced that there was no interaction between Ag NPs and RhB to form other states.

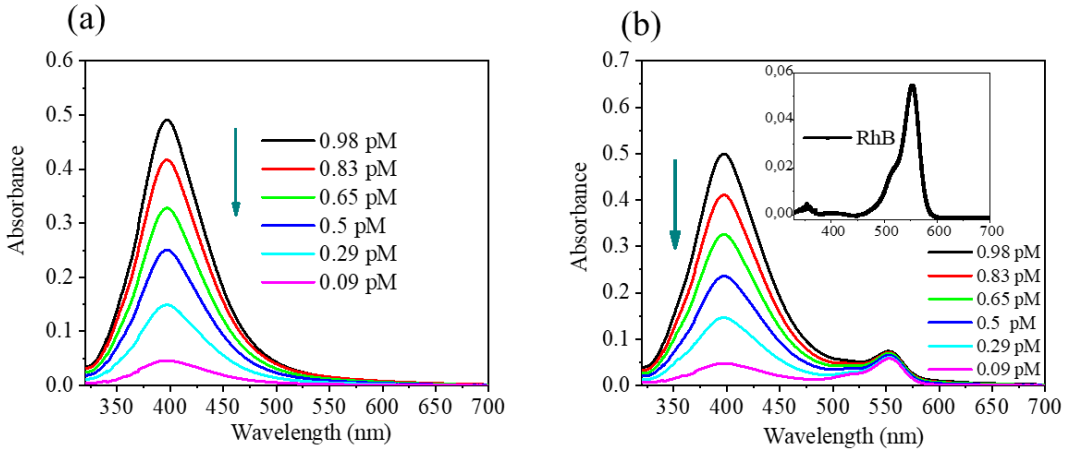

Figure 3. *Absorption spectra of various concentrations of (a) silver NPs and (b) silver NPs with the presence of RhB (0.5 µM). Inset figure: Absorption spectrum of RhB (0.5 µM)*

3.2.2. Study RhB as a fluorescent sensor for Ag NPs detection

In this work, Ag NPs were selected as an analyte to probe using RhB and acted as a fluorophore. A series of samples of mixing solutions of Ag NPs and RhB with varying Ag NPs concentrations were investigated for fluorescence properties compared with RhB under different excitation wavelengths. To examine the optimization of the detection of Ag NPs, the excitation wavelengths were carried out at eight distinct wavelengths ranging from 300 nm to 530 nm. More

specifically, wavelength excitations at 300 nm, 349 nm, 370 nm, 400 nm, 430 nm, 480 nm, 510 nm, and 530 nm were used to excite the mixing solutions of RhB and Ag NPs, with the concentration of Ag NPs varying from 0 pM to 0.98 pM. All the solutions were kept under identical conditions for fluorescence measurements under each excitation wavelength. Interestingly, the fluorescence behavior's dependence on the excitation wavelength was apparently observed. For better visualization, the dependence of the fluorescent intensity of RhB + Ag NPs solutions under three distinct excitation wavelengths at 300 nm, 400 nm, and 530 nm is plotted and presented in Figure 4.

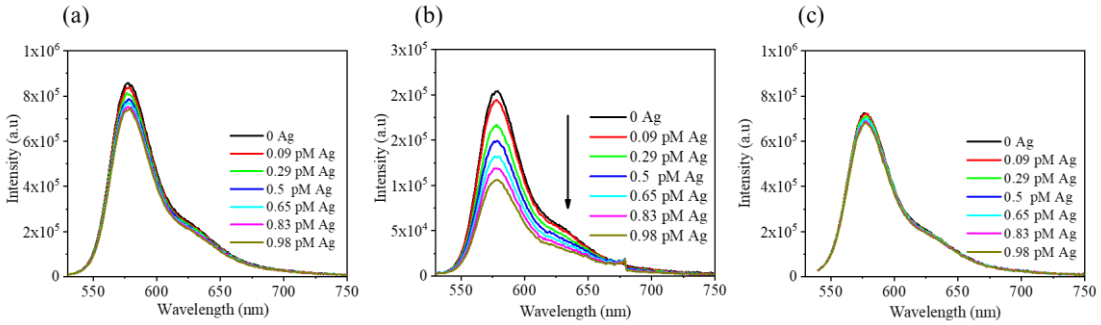

Figure 4. *Fluorescence intensity of RhB (0.5 µM) with the different concentrations of Ag NPs under excitation wavelengths at (a) 300 nm, (b) 400 nm, and (c) 530 nm*

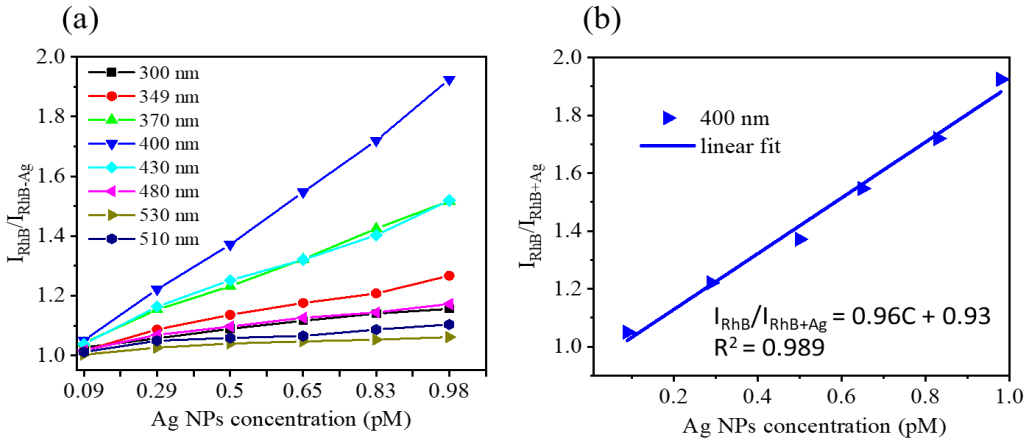

Figure 5. *(a) Calibration curves of fluorescence quenching of RhB versus the varying concentration of Ag NPs under eight different excitation wavelengths; (b) the linear fitted curve of the quenching under excitation wavelength at 400 nm*

It can be seen that the fluorescent intensity of mixing solutions of RhB + Ag NPs depends not only on the excitation wavelength but also on the concentration of Ag NPs. Figure 4 shows that the fluorescence of the mixing solutions between RhB and Ag NPs was significantly quenched under the excitation wavelength at 400 nm and was much more efficient than in the case of the excitation wavelengths at 300 nm and 530 nm. Under using excitation wavelength at 400 nm, the lowest concentration of Ag NPs could be reached of 0.09 pM, at which the fluorescent intensity of RhB + Ag NPs can still clearly distinguish from that of RhB. To confirm the optimized experimental conditions, the calibration curves under distinct excitation wavelengths (at 300 nm, 349 nm, 370 nm, 400 nm, 430 nm, 480 nm, 510 nm, and 530 nm) were plotted in Figure 5a. Upon addition of various concentrations of Ag NPs (from 0 pM ÷ 0.98 pM) into RhB solution, the fluorescent intensity of RhB decreases gradually with the increasing concentration of Ag NPs. Figure 5b indicates a good linear relationship between I_{RhB}/I_{RhB+Ag} and the concentration of Ag

NPs in the range of 0 ÷ 0.98 pM. The equation of linear regression was obtained as I_{RhB}/I_{RhB+Ag} = 0.96[Ag] + 0.93 with R^2 = 0.989. Obviously, the fluorescence system shows high sensitivity in probing Ag NPs depending on the excitation wavelength, with the limit of detection reaching 0.09 pM under excitation at 400 nm. It is a good limitation of the detection of Ag NPs compared to the previous works [8], [18].

3.2.3. Suggestion of the fluorescence quenching mechanism

It is apparent that the efficiency of fluorescence quenching of RhB with the presence of RhB depended on the excitation wavelength. The excitation wavelength at 400 nm corresponds to the highest efficiency of fluorescence quenching, and altogether, other wavelength excitations show less efficiency of fluorescence quenching. It should be noted that the excitation wavelength at 400 nm is also around the highest extinction coefficient value of Ag NPs, corresponding to the best absorption of Ag NPs. Two other excitation wavelengths at 370 nm and 430 nm indicate a relatively similar efficiency of fluorescence quenching, as presented in figure 5a. Furthermore, figure 6 illustrates that the absorbance of Ag NPs at 370 nm and 430 nm are almost identical; all other excitation wavelengths possess lower absorbance of Ag NPs. Then, it is inferred that the fluorescence quenching rests on the absorbance of the excitation wavelength of Ag NPs.

As discussed in the introduction section, the inner filter effect is an important non-irradiation fluorescence quenching process, which results from the absorption of the excitation and/or emission light by the absorber [2], [19]. As indicated above, the fluorescence quenching of RhB clearly shows the dependence on excitation wavelengths. The fluorescence quenching occurred the most significantly under the excitation wavelength of 400 nm; It could be clearly explained as the result of the absorption of excitation radiation of RhB by Ag NPs, which is known as the primary inner filter effect [2]. Therefore, the inner filter effect can be sured as the significant cause of fluorescence quenching of RhB with the presence of RhB in this case. More specifically, the high effectiveness of quenching under excitation wavelength at 400 nm could be attributed to the great value of extinction coefficient absorption of Ag NPs, which can effectively absorb excitation energy.

Furthermore, one other factor that could be counted as the cause of quenching is Forster energy transfer between Ag NPs and RhB. However, in this case, figure 6 shows the low overlap between the fluorescence spectrum of RhB and absorption of Ag NPs; thus, it can be deduced that the Forster energy transfer mechanism can be ignored in the fluorescence quenching of RhB [9].

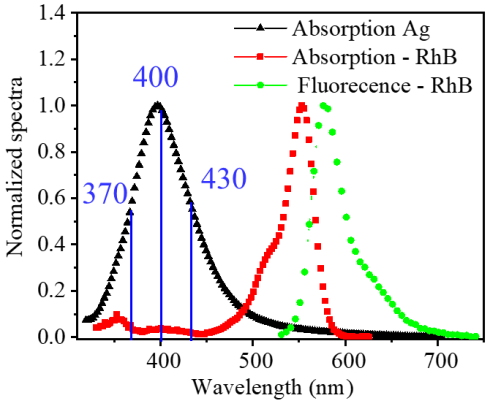

Figure 6. *The normalized absorption spectrum of silver NPs (triangle line) and normalized absorption (square line) and fluorescence (circle line) spectra of RhB*

4. Conclusion

In summary, silver NPs could be quantified and detected thanks to the fluorescence quenching of RhB. The efficiency of fluorescence quenching was proved dependent on the wavelength excitation. The lowest concentration of Ag NPs which is detected by a system composed of Ag NPs – RhB is 0.09 pM under using wavelength excitation at 400 nm. The sensitivity of the Ag NPs detection is good and comparable to previous reports. The fluorescence quenching mechanism of RhB with the presence of Ag NPs is attributed to the inner filter effect. The low concentration of detection Ag NPs might be due to the taking advantage of examination excitation wavelengths via the inner filter effect. Therefore, the examination of the fluorescence quenching dependent on wavelength excitation reveals a simple and effective method in the detection of Ag NPs.

Acknowledgments

The author would like to acknowledge the financial support of the Ministry of Education and Training of Vietnam under grand number B2023-TNA-05.

REFERENCES

[1] Z. Li, H. Lin, L. Wang, L. Cao, J. Sui, and K. Wang, "Optical sensing techniques for rapid detection of agrochemicals: Strategies, challenges, and perspectives," *Sci Total Environ,* vol. 838, no. Pt 3, Sep. 10, 2022, Art. no. 156515, doi: 10.1016/j.scitotenv.2022.156515.

[2] S. Chen, Y. L. Yu, and J. H. Wang, "Inner filter effect-based fluorescent sensing systems: A review," *Anal. Chim. Acta.,* vol. 999, pp. 13-26, Jan. 25, 2018, doi: 10.1016/j.aca.2017.10.026.

[3] B. Valeur and M. N. Berberan-Santos, *Molecular fluorescence: principles and applications*. John Wiley & Sons, 2012.

[4] J. R. Lakowicz, *Principles of fluorescence spectroscopy*. Springer, 2006.

[5] L. Shang, C. Qin, L. Jin, L. Wang, and S. Dong, "Turn-on fluorescent detection of cyanide based on the inner filter effect of silver nanoparticles," *Analyst,* vol. 134, no. 7, pp. 1477-1482, Jul. 2009, doi: 10.1039/b823471j.

[6] K. L. Kelly, E. Coronado, L. L. Zhao, and G. C. Schatz, "The optical properties of metal nanoparticles: the influence of size, shape, and dielectric environment," *J. Phys. Chem. B,* vol. 107, pp. 668-677, 2003.

[7] D. E. Charles *et al.*, "Versatile solution phase triangular silver nanoplates for highly sensitive plasmon resonance sensing," *Acs. Nano.,* vol. 4, no. 1, pp. 55-64, 2010.

[8] M. A. M. Torres, A. V. Veglia, and N. L. Pacioni, "The fluorescence quenching of rhodamine 6G as an alternative sensing strategy for the quantification of silver and gold nanoparticles," *Microchemical Journal,* vol. 160, 2021, doi: 10.1016/j.microc.2020.105645.

[9] G. R. Bardajee, Z. Hooshyar, and M. Khanjari, "Dye fluorescence quenching by newly synthesized silver nanoparticles," *Journal of Photochemistry and Photobiology A: Chemistry,* vol. 276, pp. 113-121, 2014, doi: 10.1016/j.jphotochem.2013.11.005.

[10] A. Cayuela, M. L. Soriano, and M. Valcarcel, "Reusable sensor based on functionalized carbon dots for the detection of silver nanoparticles in cosmetics via inner filter effect," *Anal. Chim. Acta,* vol. 872, pp. 70-76, May 4, 2015, doi: 10.1016/j.aca.2015.02.052.

[11] X. H. Vu *et al.*, "The sensitive detection of methylene blue using silver nanodecahedra prepared through a photochemical route," *RSC Adv.,* vol. 10, no. 64, pp. 38974-38988, Oct. 21, 2020, doi: 10.1039/d0ra07869g.

[12] S.-W. Lee *et al.*, "Effect of temperature on the growth of silver nanoparticles using plasmon-mediated method under the irradiation of green LEDs," *Materials,* vol. 7, no. 12, pp. 7781-7798, 2014.

[13] D. S. Rahman, S. Deb, and S. K. Ghosh, "Relativity of Electron and Energy Transfer Contributions in Nanoparticle-Induced Fluorescence Quenching," *The Journal of Physical Chemistry C,* vol. 119, no. 48, pp. 27145-27155, 2015, doi: 10.1021/acs.jpcc.5b08466.

[14] H. Liang, W. Wang, Y. Huang, S. Zhang, H. Wei, and H. Xu, "Controlled synthesis of uniform silver nanospheres," *The Journal of Physical Chemistry C,* vol. 114, no. 16, pp. 7427-7431, 2010.

[15] S. Mukherji, S. Bharti, G. Shukla, and S. Mukherji, "Synthesis and characterization of size- and shape-controlled silver nanoparticles," *Physical Sciences Reviews,* vol. 4, no. 1, 2019, doi: 10.1515/psr-2017-0082.

[16] D. Paramelle, A. Sadovoy, S. Gorelik, P. Free, J. Hobley, and D. G. Fernig, "A rapid method to estimate the concentration of citrate capped silver nanoparticles from UV-visible light spectra," *Analyst,* vol. 139, no. 19, pp. 4855-4861, Oct. 7, 2014, doi: 10.1039/c4an00978a.

[17] F. Khurshid, M. Jeyavelan, M. S. L. Hudson, and S. Nagarajan, "Ag-doped ZnO nanorods embedded reduced graphene oxide nanocomposite for photo-electrochemical applications," *Royal Society open science,* vol. 6, no. 2, 2019, Art. no. 181764.

[18] V. V. Koppal, R. M. Melavanki, R. A. Kusanur, and N. R. Patil, "Understanding fluorescence resonance energy transfer between biologically active coumarin derivative and silver nanoparticles using steady state and time resolved spectroscopic methods," *Journal of Molecular Liquids,* vol. 269, pp. 381-386, 2018, doi: 10.1016/j.molliq.2018.08.077.

[19] S. K. Panigrahi and A. K. Mishra, "Inner filter effect in fluorescence spectroscopy: As a problem and as a solution," *Journal of Photochemistry and Photobiology C: Photochemistry Reviews,* vol. 41, 2019, doi: 10.1016/j.jphotochemrev.2019.100318.